# p-Channel Field-Effect Transistors Based on C$_{60}$ Doped with Molybdenum Trioxide

Tae Hoon Lee,[†] Björn Lüssem,[‡,§] Kwanpyo Kim,[‡] Gaurav Giri,[‡] Yoshio Nishi,[†] and Zhenan Bao[‡,*]

[†]Department of Electrical Engineering, and [‡]Department of Chemical Engineering, Stanford University, Stanford, California 94305, United States

[§]Institut für Angewandte Photophysik, Technische Universität Dresden, George-Bähr-Str. 1, 01062 Dresden, Germany

Ⓢ *Supporting Information*

ABSTRACT: Fullerene (C$_{60}$) is a well-known n-channel organic semiconductor. We demonstrate that p-channel C$_{60}$ field-effect transistors are possible by doping with molybdenum trioxide (MoO$_3$). The device performance of the p-channel C$_{60}$ field-effect transistors, such as mobility, threshold voltage, and on/off ratio is varied in a controlled manner by changing doping concentration. This work demonstrates the utility of charge transfer doping to obtain both n- and p-channel field-effect transistors with a single organic semiconductor.
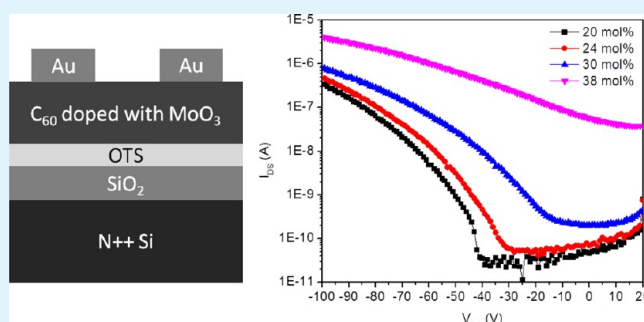
Organic semiconductors have been much studied because of their potential for many applications in low-cost, large-area, and flexible electronics.[1−5] It is desirable to use complementary metal-oxide-semiconductor(CMOS) technology for digital integrated circuits. CMOS dominates in inorganic semiconductor integrated circuits due to its scalability, high noise immunity, and low static power dissipation.[6] However, implementation of CMOS with organic semiconductors requires both n- and p-channel field-effect transistors. The most common approach is to pattern two types of field-effect transistors fabricated with two different organic semiconductor materials.[7−10] The fabrication process is more complicated and costly than that with a single semiconductor. To address this problem, ambipolar materials have been used.[11,12] However, it is difficult to realize high on/off ratios for such materials.[11,12] Alternatively, doping an organic semiconductor to achieve both n- and p-channel field-effect transistors has been explored.[13,14] For example, pentacene, a popular organic semiconductor for p-channel field-effect transistors, was reported to be used for n-channel field-effect transistors by doping dielectric-semiconductor interface and contacts with Ca.[13]

Fullerene (C$_{60}$) is a high mobility organic semiconductor for n-channel field-effect transistors. Previously, we demonstrated improved air stability of C$_{60}$-based n-channel field-effect transistors.[15,16] However, no p-channel field-effect transistors based on C$_{60}$ has been reported. Because C$_{60}$ has a highly deeply-lying highest occupied molecular orbital (HOMO) level of 6.4 eV,[17] p-type doping C$_{60}$ is much more difficult than other organic semiconductors with higher HOMO levels. Transition metal oxides, such as molybdenum trioxide (MoO$_3$), have been recently studied as a p-type dopant for organic semiconductors
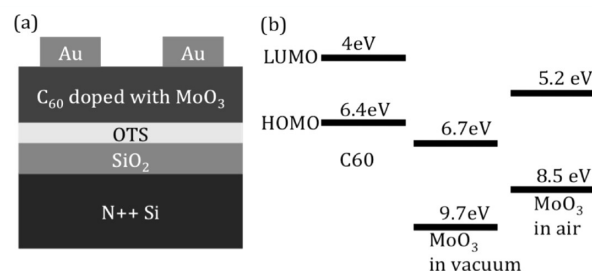

Figure 1. (a) Schematic structure of field-effect transistors and (b) energy levels for C$_{60}$ and MoO$_3$ in vacuum and in air (MoO$_3$ energy values taken from refs 19 and 22).

due to their high electron affinity.[17−22] MoO$_3$ was initially known to have an electron affinity of 2.3 eV,[23,24] but ultraviolet and inverse photoemission spectroscopy (UPS/IPES) measurements in ultra high vacuum (UHV) revealed a large electron affinity of MoO$_3$ to be 6.7 eV.[18−21] The high electron affinity of MoO$_3$ makes it possible to p-dope C$_{60}$. Indeed, it was previously reported that coevaporation of MoO$_3$ with C$_{60}$ shifted the Fermi level of C$_{60}$ toward its HOMO.[17] The Fermi level shift was measured with a Kelvin probe and confirmed by the different band bending location in undoped C$_{60}$ and doped C$_{60}$ photovoltaic cells. Also, solar cells based on the homojunction
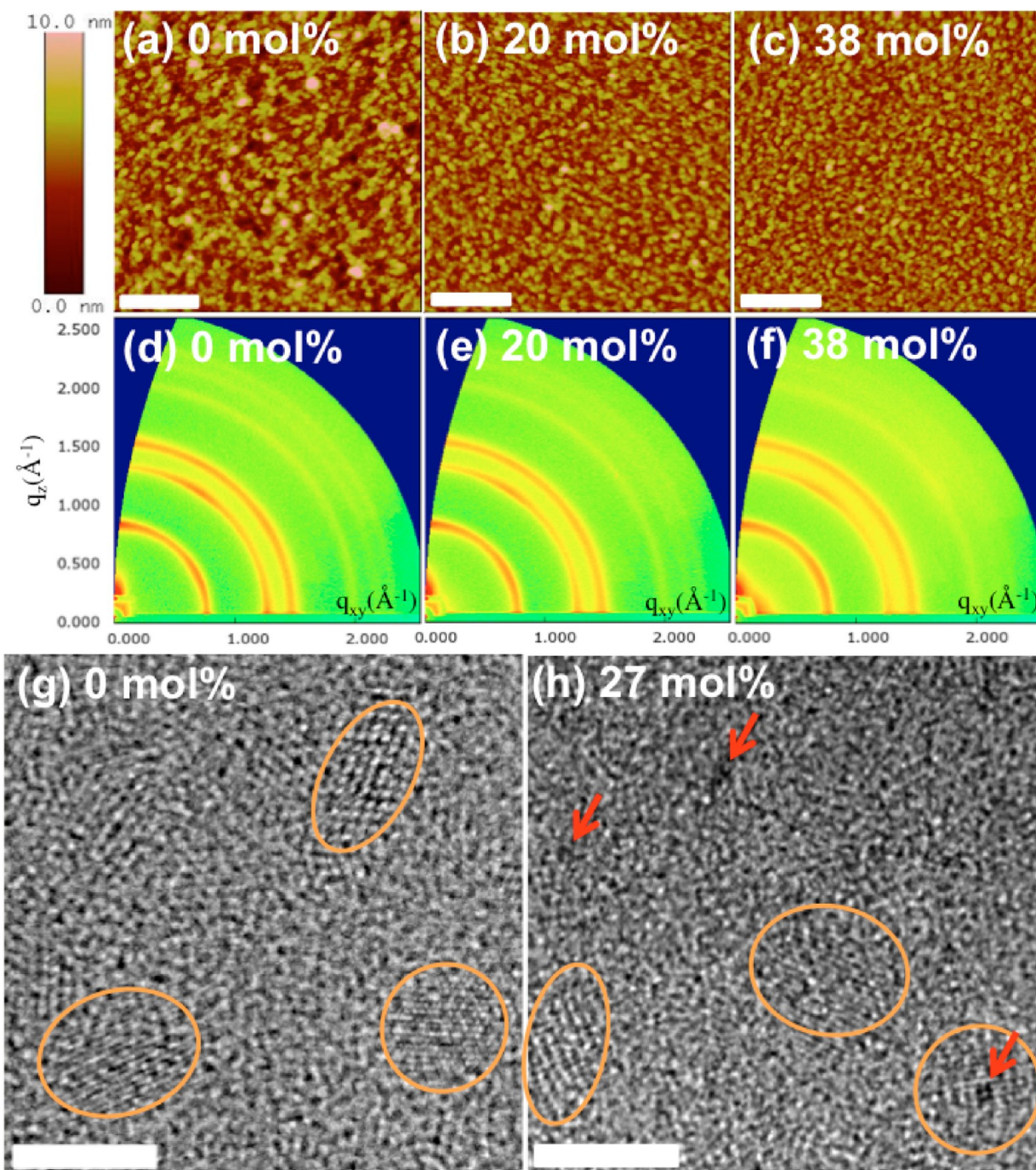
Figure 2. AFM images for (a) 0 mol % (undoped), (b) 20 mol %, (c) 38 mol % C_{60}:MoO_3 with scale bars of 250 nm. GIXD results for (d) 0 mol %, (e) 20 mol %, (f) 38 mol % C_{60}:MoO_3. TEM images for (g) 0 mol %, (h) 27 mol % C_{60}:MoO_3 grown on amorphous carbon TEM grid with scale bars of 10 nm. Orange colored circles and black spots indicate C_{60} crystallites and MoO_3, respectively.

of MoO_3 doped C_{60} and Ca doped C_{60} were demonstrated.[25] In this letter, we show that it is possible to realize p-channel field-effect transistors by doping C_{60} with MoO_3. The device performance can be controlled by doping concentrations. This work indicates the doping is an effective method to tune charge carrier transport type in field-effect transistors.

In order to build the field-effect transistors, we used highly n-doped silicon substrate as a back gate and a thermally grown SiO_2 (300 nm) as a dielectric as illustrated in Figure 1. The silicon dioxide layer was treated with a crystalline octadecyltrimethoxysilane- (OTS) self-assembled-monolayer (SAM) according to procedures

reported before in order to effectively reduce interface traps at the SiO_2–C_{60} interface and also to facilitate 2D crystal growth of C_{60}.[26,27] For control samples, a C_{60} (21 nm) layer was evaporated on top of the OTS treated SiO_2 held at room temperature at a deposition rate of 0.25 Å/s. For doped samples, C_{60} was coevaporated with MoO_3 at various doping concentrations from 11 to 39 mol %. We note that the concentration of MoO_3 used here is much higher than the typical dopant concentrations used in inorganic semiconductors. However, the roles of MoO_3, tuning conduction type and conduction level, are similar to those of conventional dopants. Therefore, we still

used the term "doping" in this case. Gold electrodes (40 nm) were then evaporated through a shadow mask on the undoped and doped C_{60} layers as drain and source contacts. The channel length and width of the field-effect transistors are 50 um and 1000 um, respectively. In order to study the effects of contact doping and compare it with coevaporation, 3 nm MoO_3 followed by 40 nm Au was evaporated on the undoped 21 nm thick C_{60} layer for some samples. For transmission electron microscopy(TEM) measurements, an intrinsic C_{60} film (10 nm) and a 27 mol % doped C_{60} film (10 nm) were evaporated on thin (~10 nm) amorphous carbon TEM grids.

After the fabrication, we performed atomic force microscopy-(AFM), grazing incidence X-ray diffraction(GIXD), and high resolution TEM imaging to investigate the effects of MoO_3 into the C_{60} matrix during coevaporation and the results are shown in Figure 2. Figures 2b, c, e, f indicate that the grain size and crystallinity of the doped films do not change significantly at doping concentrations on the order of 20−38 mol %. However, the doped C_{60} grains are slightly smaller than the undoped C_{60} grains as shown in Figure 2a−f and Table 1. The grain sizes for

Table 1. C_{60} Crystallite Sizes Vs Doping Concentrations from GIXD Results

doping concentration (mol %)	Bragg peak q_{xy} ($Å^{-1}$)	fwhm ($Å^{-1}$)	grain size (nm)
0	0.782	0.0687	9.14
20	0.786	0.0750	8.37
24	0.783	0.0787	7.98
30	0.785	0.0852	7.37
38	0.784	0.0745	8.43

films doped at various concentrations were calculated using full width at half-maximum(fwhm) values from GIXD images as listed in Table 1.[28] In Table 1, the calculated sizes of C_{60} grains without doping are almost the same as those of doped C_{60} films, only larger by 1−2 nm. Also, the C_{60} grain size on the OTS self-assembled monolayer is similar as that grown on the amorphous carbon of the TEM as seen in Figure 2g. The orange colored ellipses in panels g and h in Figure 2 represent the C_{60} grains, whereas the dark spots are MoO_3. A TEM image for 27 mol % doped C_{60} on the amorphous carbon of a TEM grid is shown in Figure 2h. In the TEM image, we find that MoO_3 dopants are evenly distributed through the coevaporated C_{60} film. Moreover, the observed MoO_3 within a C_{60} grain suggests the low possibility of dopants segregation to grain boundaries of C_{60}. AFM and GIXD images for other doping concentrations and original large images for Figure 2g and h are provided in Figures S1−S4 in the Supporting Information.

The transfer characteristics of the undoped and doped C_{60} field-effect transistors are compared in Figure 3. They were measured in a nitrogen atmosphere with a Keithley 4200-SCS parameter analyzer. For each MoO_3 concentration, we have measured seven devices and obtained average mobilities, threshold voltages, and on/off ratios. Mobility was extracted from the highest slope of $\sqrt{I_{DS}}$ vs V_{GS} curve in the saturation regime. The threshold voltage was subsequently obtained by linear extrapolation at the V_{GS} of the highest slope. Field-effect transistors based on undoped C_{60} showed n-type conduction with a field-effect mobility of 0.12 (±0.047) $cm^2V^{-1}s^{-1}$, a threshold voltage of 62.8 (±3.81) V, and an on/off ratio of 4.14 (±1.68)x10^5 as shown in Figure 3a. This is similar to those reported for undoped C_{60} field-effect transistors deposited at a
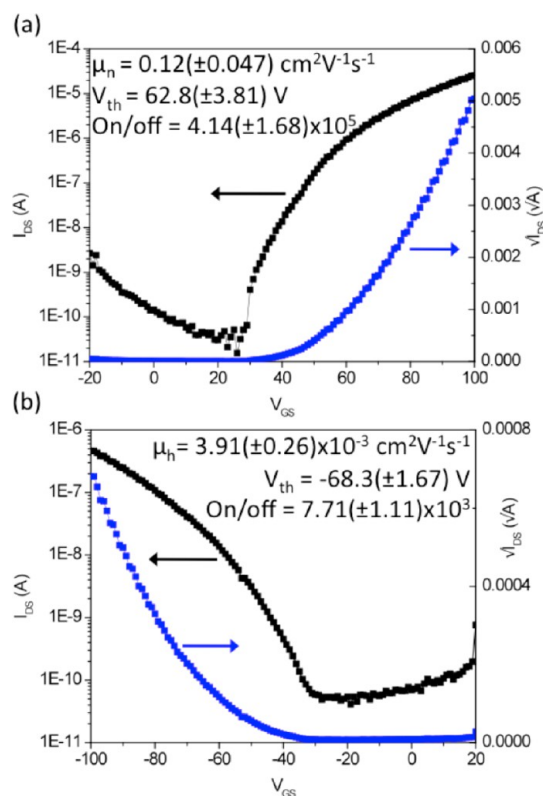

Figure 3. (a) n-type conduction in undoped C_{60} at V_{DS} = 100 V (b) p-type conduction in MoO_3-doped C_{60} at V_{DS} = −100 V.

substrate temperature held at room temperature.[29] However, when C_{60} was doped with MoO_3 at ≥8−9 mol % by coevaporation, p-type conduction was observed. As an example, the current−voltage characteristics for 24 mol % doped C_{60} transistors are illustrated in Figure 3b in which the negative biased gate voltage resulted in increased absolute value of the negative drain-source current with a negative applied drain-source voltage. Therefore, by doping with MoO_3, C_{60}, a well-known n-type organic semiconductor, can exhibit p-type conduction. MoO_3 is likely to have two functions: dopes C_{60} by generating excess hole charge carriers and passivates hole traps. Field-effect transistors based on the 24 mol % doped C_{60} exhibit a field-effect mobility of 3.91 (±0.26) × 10^{-3} cm^2 V^{-1} s^{-1}, a threshold voltage of −68.3 (±1.67) V, and an on/off ratio of 7.71 (±1.11) × 10^3.

The device performance of doped C_{60} field-effect transistors, such as mobility, threshold voltage, and on/off ratio, is controllable by changing the doping concentration as shown in Figure 4. As doping concentration increased from 11 to 39 mol %, average hole mobility also increased from $1.52 × 10^{-3}$ to $5.61 × 10^{-3}$ cm^2 V^{-1} s^{-1} with the maximum of $8.51 × 10^{-3}$ cm^2 V^{-1} s^{-1}. At doping concentrations of 8−9 mol %, devices showed p-type conduction only with hole mobility of the order of $1 × 10^{-6}$ to $1 × 10^{-5}$ cm^2 V^{-1} s^{-1}. As the doping concentration decreases further, p-type conduction disappears and n-type conduction of C_{60} starts to appear. In our experiment, devices based on 3 mol % doped C_{60} showed n-type conduction only. The magnitude of threshold voltage decreased with increasing doping concentration because the holes generated by MoO_3 dopants helped formation of an electrical channel at a lower negative gate voltage. Both on-state and off-state currents rose with increasing doping concentration but the increase in off-state
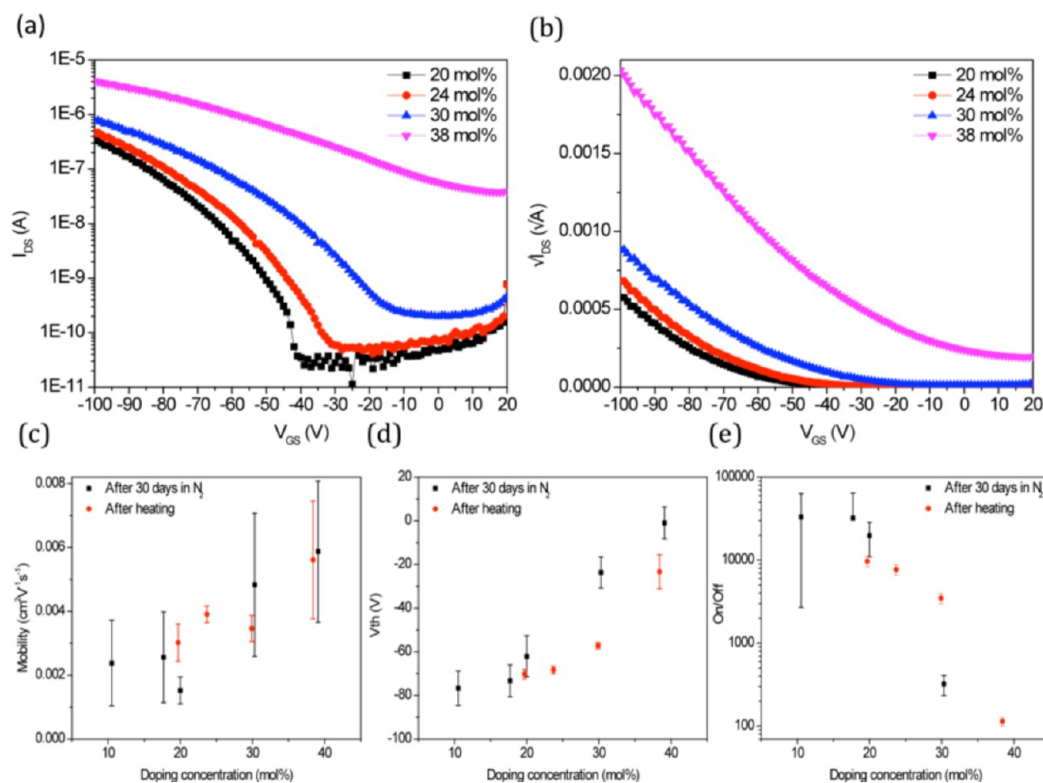
2339

dx.doi.org/10.1021/am3026568 | ACS Appl. Mater. Interfaces 2013, 5, 2337−2341

Figure 4. (a) I_{DS} vs V_{GS} at $V_{DS} = -100$ V; (b) $\sqrt{I_{DS}}$ vs V_{GS} at $V_{DS} = -100$ V; (c) mobility; (d) threshold voltage; (e) on/off ratio vs doping concentrations.

current was larger than that in on-state current, resulting in the decrease in on/off ratio. We observed that the maximum average on/off ratio of 3.31×10^4 was achieved at low doping concentrations. Our observation that the off-current significantly increased with high concentrations of MoO_3 suggests that charge transfer doping from MoO_3 to C_{60} is indeed taking place instead of a purely trap-filling mechanism as observed from other systems.[30]

The enhanced hole mobility with increasing doping concentration can be explained by the increased hole concentration filling traps in the doped C_{60} film as doping concentration increases. AFM and Grazing Incidence X-ray Diffraction (GIXD) analyses in Figure 2 and Table 1 show that doped films have similar grain sizes and crystallinity at doping concentrations of 20−38 mol %, which indicates that the change in mobility at different doping concentrations is not ascribed to the change in grain size or crystallinity, but mainly to the change in hole concentration generated by MoO_3 dopants. The hole mobilities in the doped C_{60} films at various doping concentrations are more than 1 order of magnitude lower than the electron mobility in n-channel field-effect transistors based on undoped C_{60}. The low hole mobility can be attributed to two possible reasons. First, the doping with MoO_3 introduces structural defects in C_{60} films that may reduce the hole mobility. Figure 2 and Table 1 show that the average grain size in doped C_{60} is slightly smaller than that in undoped C_{60} by about 1−2 nm, which suggests that doping affects the growth of C_{60} and may create defects in C_{60} film. Another possible reason is that the HOMO level of C_{60} is so deep that the holes may be readily trapped by defects and impurities.

To confirm that the p-type conduction is not solely due to doping at the drain and source contacts, we tested the devices with an intrinsic C_{60} layer and MoO_3(3 nm)/Au(40 nm) top contacts. The transfer curves of these devices show significantly

reduced p-type conduction as shown in Figure S5 in the Supporting Information, which indicates that p-type conduction in doped C_{60} is mainly due to bulk doping, but not contact doping. Therefore, bulk-doping by coevaporation is crucial for p-type conduction in C_{60} field-effect transistors.

For most p-channel organic transistors, exposure to air results in a slight increase in charge carrier mobility due to slight p-doping by oxygen. Interestingly, the MoO_3-doped C_{60} field-effect transistors did not show any field-effect current when measured in air whereas they exhibited p-type conduction when stored back in a nitrogen atmosphere. The drain current level increased with the storage time in a nitrogen atmosphere for a week. This change in device characteristics resulted from a reversible change in energy levels of MoO_3 depending on its atmosphere. The energy levels of MoO_3 rise upon exposure to air during fabrication process and drop back down when oxygen and water vapors in the doped C_{60} films are gradually removed in the dry nitrogen atmosphere as displayed in Figure 1b.[22] In air, the LUMO of MoO_3 higher than the HOMO of C_{60} prevents p-type doping, which was why the transistors did not show any field-effect current. As the devices were stored in a nitrogen atmosphere, the energy levels of MoO_3 are recovered leading to p-type conduction as demonstrated in Figure 5a. Instead of storing samples in nitrogen for a few days, heating samples in nitrogen at 100 °C for 2h accelerated the removal of oxygen and water vapors from the C_{60} layer. After heating, more MoO_3 dopants recovered their energy levels[22] and thus drain current level increased as shown in Figure 5b. Annealing effect on MoO_3 was also studied by M. C. Gwinner et al.[22] Therefore, the transfer curves for field-effect transistors in panels a and b in Figure 4 were all measured after heating.

In conclusion, we have demonstrated p-channel field-effect transistors by doping C_{60} with MoO_3. Therefore, both n- and
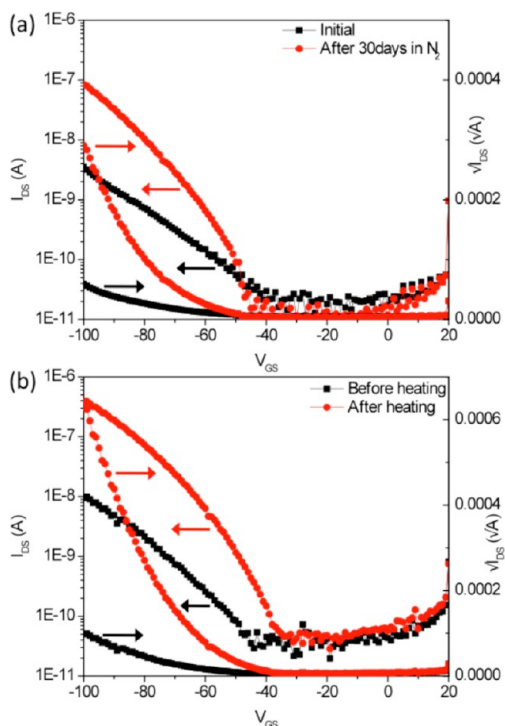
2340

dx.doi.org/10.1021/am3026568 | ACS Appl. Mater. Interfaces 2013, 5, 2337−2341

Figure 5. (a) Transfer characteristics of initial and stored samples in N_2 for 30 days, $V_{DS} = -100$ V, 20 mol % C_{60}:MoO_3, (b) transfer characteristics before and after heating at 100 °C for 2 h, $V_{DS} = -100$ V, 24 mol % C_{60}:MoO_3.

p-channel field-effect transistors can be built with a single organic semiconductor, C_{60}. Device performances of the doped field-effect transistors can be manipulated by varying doping concentration, which would be an important feature when device characteristics need to be tuned for individual applications. This work demonstrates doping is a useful method to tune the conduction type and performance in organic semiconductor devices. This also broadens the availability of various types of organic semiconductors.

ASSOCIATED CONTENT

Ⓢ Supporting Information
AFM topography images (Figure S1) and grazing incidence X-ray diffraction (GIXD) patterns (Figure S2) at various doping concentrations. TEM images for 0 mol % C_{60} (Figure S3) and 27 mol % C_{60}:MoO_3 (Figure S4). Transfer curves for devices with contact doping (Figure S5). This material is available free of charge via the Internet at http://pubs.acs.org.

AUTHOR INFORMATION

Corresponding Author
*E-mail: zbao@stanford.edu.

Notes
The authors declare no competing financial interest.

ACKNOWLEDGMENTS

REFERENCES

(1) Arias, A. C.; MacKenzie, J. D.; McCulloch, I.; Rivnay, J.; Salleo, A. *Chem. Rev.* **2010**, *110*, 3−24.
(2) Klauk, H. *Chem. Soc. Rev.* **2010**, *39*, 2643−2666.
(3) Someya, T.; Sekitani, T.; Iba, S.; Kato, Y.; Kawaguchi, H.; Sakurai, T. *Proc. Natl. Acad. Sci. U. S. A.* **2004**, *101*, 9966−9970.
(4) Rogers, J. A.; Someya, T.; Huang, Y. *Science* **2010**, *327*, 1603−1607.
(5) Sokolov, A. N.; Tee, B. C.-K.; Bettinger, C. J.; Tok, J. B.-H.; Bao, Z. *Acc. Chem. Res.* **2012**, *45*, 361−371.
(6) Weste, N. H. E.; Eshraghian, K. *Principles of CMOS VLSI Design: a Systems Perspective*, 1st ed.; Addison-Wesley: Boston, 1985; Vol. *854*.
(7) Dodabalapur, A.; Laquindanum, J.; Katz, H. E.; Bao, Z. *Appl. Phys. Lett.* **1996**, *69*, 4227−4229.
(8) Klauk, H.; Zschieschang, U.; Pflaum, J.; Halik, M. *Nature* **2007**, *445*, 745−748.
(9) Yan, H.; Chen, Z.; Zheng, Y.; Newman, C.; Quinn, J. R.; Dötz, F.; Kastler, M.; Facchetti, A. *Nature* **2009**, *457*, 679−686.
(10) Li, H.; Tee, B. C.-K.; Giri, G.; Chung, J. W.; Lee, S. Y.; Bao, Z. *Adv. Mater.* **2012**, *24*, 2588−2591.
(11) Zaumseil, J.; Sirringhaus, H. *Chem. Rev.* **2007**, *107*, 1296−1323.
(12) Meijer, E. J.; De Leeuw, D. M.; Setayesh, S.; Van Veenendaal, E.; Huisman, B. H.; Blom, P. W. M.; Hummelen, J. C.; Scherf, U.; Klapwijk, T. M. *Nat. Mater.* **2003**, *2*, 678−682.
(13) Ahles, M.; Schmechel, R.; Von Seggern, H. *Appl. Phys. Lett.* **2004**, *85*, 4499−4501.
(14) Schmechel, R.; Ahles, M.; Von Seggern, H. *J. Appl. Phys.* **2005**, *98*, 084511.
(15) Wei, P.; Oh, J. H.; Dong, G.; Bao, Z. *J. Am. Chem. Soc.* **2010**, *132*, 8852−8853.
(16) Wei, P.; Menke, T.; Naab, B. D.; Leo, K.; Riede, M.; Bao, Z. *J. Am. Chem. Soc.* **2012**, *134*, 3999−4002.
(17) Kubo, M.; Iketaki, K.; Kaji, T.; Hiramoto, M. *Appl. Phys. Lett.* **2011**, *98*, 073311.
(18) Kröger, M.; Hamwi, S.; Meyer, J.; Riedl, T.; Kowalsky, W.; Kahn, A. *Appl. Phys. Lett.* **2009**, *95*, 123301.
(19) Kröger, M.; Hamwi, S.; Meyer, J.; Riedl, T.; Kowalsky, W.; Kahn, A. *Org. Electron.* **2009**, *10*, 932−938.
(20) Irfan; Ding, H.; Gao, Y.; Kim, D. Y.; Subbiah, J.; So, F. *Appl. Phys. Lett.* **2010**, *96*, 073304.
(21) Irfan; Ding, H.; Gao, Y.; Small, C.; Kim, D. Y.; Subbiah, J.; So, F. *Appl. Phys. Lett.* **2010**, *96*, 243307.
(22) Gwinner, M. C.; Di Pietro, R.; Vaynzof, Y.; Greenberg, K. J.; Ho, P. K. H.; Friend, R. H.; Sirringhaus, H. *Adv. Funct. Mater.* **2011**, *21*, 1432−1441.
(23) Reynolds, K. J.; Barker, J. a.; Greenham, N. C.; Friend, R. H.; Frey, G. L. *J. Appl. Phys.* **2002**, *92*, 7556−7563.
(24) Chu, C.-W.; Li, S.-H.; Chen, C.-W.; Shrotriya, V.; Yang, Y. *Appl. Phys. Lett.* **2005**, *87*, 193508.
(25) Kubo, M.; Kaji, T.; Hiramoto, M. *AIP Advances* **2011**, *1*, 032177.
(26) Ito, Y.; Virkar, A.; Bao, Z. *J. Am. Chem. Soc.* **2009**, *131*, 9396−9404.
(27) Virkar, A.; Mannsfeld, S.; Oh, J. H.; Toney, M. F.; Tan, Y. H.; Liu, G.; Scott, J. C.; Miller, R.; Bao, Z. *Adv. Funct. Mater.* **2009**, *19*, 1962−1970.
(28) Smilgies, D. *J. Appl. Crystallogr.* **2009**, *42*, 1030−1034.
(29) Singh, T. B.; Sariciftci, N. S.; Yang, H.; Yang, L.; Plochberger, B.; Sitter, H. *Appl. Phys. Lett.* **2007**, *90*, 213512.
(30) Walzer, K.; Maennig, B.; M. Pfeiffer, A.; Leo, K. *Chem. Rev.* **2007**, *107*, 1233−1271.